A stochastic fire-diffuse-fire model with realistic cluster dynamics.

Ana Calabrese[1,4], Daniel Fraiman [2], Daniel Zysman [3], and Silvina Ponce Dawson [1]
[1] *Departamento de Física, FCEN-UBA, Ciudad Universitaria, Pabellón I, (1428) Buenos Aires, Argentina*
[2] *Departamento de Matemática y Ciencias, Universidad de San Andrés, Buenos Aires, Argentina*
[3] *Department of Biology and Centre for Neural Dynamics, University of Ottawa, 30 Marie-Curie, Ottawa, Ontario, K1N 6N5, Canada* [4] *Center for Theoretical Neuroscience, Columbia University, 1051 Riverside Dr., New York, NY, USA*

(Dated: July 20, 2010)

Living organisms use waves that propagate through excitable media to transport information. Ca^{2+} waves are a paradigmatic example of this type of processes. A large hierarchy of Ca^{2+} signals that range from localized release events to global waves has been observed in *Xenopus laevis* oocytes. In these cells, Ca^{2+} release occurs trough inositol 1,4,5-trisphosphate receptors (IP_3Rs) which are organized in clusters of channels located on the membrane of the endoplasmic reticulum. In this article we construct a stochastic model for a cluster of IP_3R's that replicates the experimental observations reported in Fraiman *et al*, *Biophys. J.* **90**, 3897 (2006). We then couple this phenomenological cluster model with a reaction-diffusion equation, so as to have a discrete stochastic model for calcium dynamics. The model we propose describes the transition regimes between isolated release and steadily propagating waves as the IP_3 concentration is increased.

PACS numbers: 87.16.-b 87.16.Xa 87.16.A- 87.10.Mn

I. INTRODUCTION

Oscillations and waves in the concentration of free intracellular calcium (Ca^{2+}) are seen in a variety of cells and are known to be an important intra and intercellular signaling system [1]. It is thus of interest to determine the mechanisms underlying such complex dynamic behavior. In many cell types, a key component of this signaling pathway is the inositol triphosphate receptor (IP_3R), which is also a Ca^{2+} channel. The spatiotemporal properties of signals arising through IP_3R's have been extensively characterized by optical imaging in *Xenopus laevis* oocytes [2]. In these cells, Ca^{2+} imaging techniques have revealed that the cytoplasm does not act as a continuous, homogeneous excitable medium. Instead, Ca^{2+} liberation occurs at discrete functional release sites spaced a few micrometers apart, composed of several clustered IP_3R's [2–8]. The open probability of IP_3R's depends on both the IP_3 and cytosolic Ca^{2+} concentrations [9, 10]. A key feature, is the well-established biphasic action of Ca^{2+} in both facilitating and inhibiting the opening of IP_3R's, through which Ca^{2+} is liberated into the cytosol. For relatively low $[Ca^{2+}]$, the Ca^{2+} released by one channel increases the open probability of neighboring channels, whereas at high $[Ca^{2+}]$, it inhibits the channels and terminates the release [11–15]. This dependence of the open probability of the release channels on cytosolic Ca^{2+} creates communication between channels.

As a result of the combination of the channels spatial organization and of the process of Ca^{2+}-induced Ca^{2+} release (CICR)([16–18]), cytosolic Ca^{2+} signals in oocytes display a hierarchical spatio-temporal organization spanning over six orders of magnitude, which include Ca^{2+} "blips" that represent the release of Ca^{2+} through a single or a few IP_3R's ([4, 19, 20]), "puffs" that involve the concerted opening of several IP_3R's in a cluster ([4, 20–22]) and Ca^{2+} waves that propagate globally across the cell by successive cycles of CICR and Ca^{2+} diffusion between clusters ([21–23]). Ca^{2+} puffs reflect the dynamics of IP_3R's within a cluster. This dynamics is ruled by the kinetics of each channel and by the interaction among them due to the spatiotemporal Ca^{2+} distribution on the nanometer scale.

Several mathematical models have been proposed to describe Ca^{2+} release through clustered IP_3R's. The approaches vary depending on the spatial and time scale that they try to resolve. The dynamics of localized signals such as puffs has been simulated with models that include a detailed stochastic description of the channels in the cluster and which resolve distances on the nm scale [5, 7]. Using this fine spatial resolution and the characteristic time scale of single channel transitions ($\sim ms$) to describe Ca^{2+} waves which travel mm distances and last for hundreds of seconds is computationally expensive [5, 24]. For this reason, mathematical models of this type of global signals involve different approximations. For some time most such models were deterministic (see *e.g.* [25]) while stochastic models were left to account for local signals such as puffs [5, 18, 26–28]. It is currently clear, however, that stochastic effects are not only relevant for local release events but are a fundamental aspect of the Ca^{2+} dynamics for the full range of observed signals, including waves [29–34]. Efficient modeling strategies are necessary to include the intrinsic stochasticity of Ca^{2+} global signals describing, at the same time, the largest scales involved. Some of the approaches presented in the literature assumed that clustered IP_3R's are in such close contact that $[Ca^{2+}]$ could be considered homogeneous throughout the cluster [26, 35–39]. This type of models can be further simplified

as done in [40, 41], where it is assumed that $[Ca^{2+}]$ at one cluster depends only on the number of nearest release sites where there are open channels and that each neighboring (active) site adds a time-independent contribution to $[Ca^{2+}]$. Some years ago a finite element hybrid scheme was introduced to resolve the spatial gradients close to a channel and simulate calcium signals efficiently [42]. The algorithm was used to simulate local signals. More recently, we introduced a model that resolves the dynamics of Ca^{2+} in the intra-cluster region using a fine grid and some simplifications [43]. The dynamics in the region outside the cluster is described on a coarser spatial resolution. Coupling both regions, the model is able to span several orders of magnitude in space and time in an efficient way. The use of a master equation to describe the Ca^{2+} puff dynamics as introduced in [31] also provides an efficient way to deal with the multiple scales that are inherent to Ca^{2+} signals.

The models mentioned so far use some kinetic model to describe the transitions between conformational states of single IP_3R's. There is some controversy on how single IP_3R's behave [13, 15]. Consequently, there is a variety of IP_3R kinetic models [44–47] and it is not completely clear which one describes the behavior of the channel under the conditions encountered in intact cells. In particular, Ca^{2+} is not used as the carrier in most electrophysiology experiments [15] to prevent the feedback that the released Ca^{2+} can have on the kinetics of the channel. Optical techniques allow the direct study of IP_3R's in their native environment. However, there is less control on the concentrations of IP_3 and Ca^{2+} to which the channels are subjected. This, together with the clusterization of the channels makes it difficult to infer a single IP_3 kinetic model from optical images of Ca^{2+} signals in intact cells.

The observation that global intracellular Ca^{2+} oscillations are the result of (local) random Ca^{2+} spikes which involve Ca^{2+} release from one or several channels in a cluster [29] indicates that IP_3R clusters constitute a basic component of Ca^{2+} signals [31]. This is further supported by obsevarations which indicate that IP_3R's are densely packed inside clusterst [48]. One way to overcome the lack of an IP_3R kinetic model that can readily be applied under physiological conditions is then to describe Ca^{2+} wave propagation using IP_3R clusters as the units of Ca^{2+} release. This approach is similar, in spirit, to the "fire-diffuse-fire" model [49–51], where the Ca^{2+} release sites are point sources separated by the typical mean inter-cluster distance. The model of [31] also uses clusters as basic release units but the description of their dynamics still needs an IP_3R kinetic model. One of the drawbacks of the original "fire-diffuse-fire" model is that it treats Ca^{2+} release in a deterministic way: a site starts to release Ca^{2+} whenever $[Ca^{2+}]$ at the site exceeds a fixed threshold. This simple description of CICR has been relaxed in a stochastic version of the "fire-diffuse-fire" model [52, 53] in which the threshold is assumed to be a random variable with a certain distribution. In the present paper we follow a more realistic approach. More specifically, we use puff information to construct a phenomenological stochastic model of a cluster as a whole which reproduces the main properties of experimentally observed puffs. We then use this heuristic model to describe the dynamics of the localized Ca^{2+} release sites in a modified version of the "fire-diffuse-fire model" with which we simulate the observed range of Ca^{2+} signals, *i.e.*, from blips to waves. The model thus constructed gives a more realistic description of the transition from localized to global signals and of propagation failure than the original "fire-diffuse-fire" model and the stochastic extension of [52], keeping their simplicity to a great extent. As in the original "fire-diffuse-fire" model, the stochastic version we test in the present paper simulates the dynamics of the released Ca^{2+} in terms of an effective diffusion coefficient. We discuss, however, how the effective cluster model may be used within a more realistic description of this dynamics to study global Ca^{2+} signals in a way that would be less expensive than using the approaches of [43, 54].

The organization of the paper is as follows. In Sec. II we describe how we construct our effective cluster model. In Sec. III we choose the parameters of the model based on a subset of the observations analyzed in [55]. In Sec. IV we compare the amplitude and inter-puff time distributions obtained with the model with those observed experimentally [55] and show that they are statistically equivalent. We also discuss how and which properties of the cluster should be changed in the presence of different types of buffers. In Sec. V we present our stochastic version of the "fire-diffuse-fire" model in which each release site is simulated using the effective cluster model of the previous section. We also show the result of some simulations. In particular, we show that the model is able to simulate the transition from puffs to abortive waves to steady waves. We discuss possible improvements and further uses of the effective cluster model and summarize the results in Sec. VI.

II. HEURISTIC CLUSTER MODEL

In this Section we describe how we use the experimental observations analyzed in [55] to construct an effective cluster model and determine numerical values for its parameters. These observations were obtained in *Xenopus laevis* oocytes in which $270\mu M$ of the exogenous Ca^{2+} buffer, EGTA, had been added to prevent Ca^{2+} wave propagation. The images were obtained using confocal microscopy, $40\mu M$ of the fluorescent Ca^{2+} dye Oregon Green 488 BAPTA 1 and a continuous photorelease of IP_3 to evoke the signals. The experimental histograms of puff amplitude, A, interpuff time, τ, and puff duration show that they all vary from event to event even at the same release site. The variability of the last two quantities can be incorporated into a Markovian model in which the cluster can be in a finite set of states and

make stochastic transitions among them. This type of approach would require the existence of many open states in order to reproduce the amplitude variability observed at each site. In this paper we follow a different approach: we build a phenomenological cluster kinetic model in which the transitions into and out of the open states are treated as if there was only one open state. The current that flows through the channel when it is open, on the other hand, is a random variable that is drawn from a continuous distribution that depends on cytosolic Ca^{2+}. In this way we mimic the puff amplitude variability as explained later in more detail. In the case of the time the cluster remains "open", we try different possibilities, some of which involve choosing this time from a prescribed distribution.

A. Cluster kinetic model

The observed distribution functions of A and τ, by themselves, do not provide enough information to decide how the transitions of the kinetic model are calcium-regulated. Taking into account that Ca^{2+}-mediated coupling between clusters is not present in the experiments analyzed in [55], the calcium concentration in the vicinity of a cluster after a release event has finished is directly related to the amplitude of the event. The calcium concentration before the occurrence of a puff, on the other hand, depends on the time that has elapsed since the previous release event at the same site has occurred (the inter-puff time). Thus, by studying the correlation between puff amplitudes and interpuff times it is possible to extract information on the effect of cytosolic Ca^{2+} on the dynamics that is useful for the construction of the phenomenological model. The data presented in [55] show that the amplitude (interpuff time) distributions conditioned to large or small previous interpuff times (amplitudes) are different and reveal that the Ca^{2+} released through the channels in a cluster plays mainly an inhibitory role on the subsequent behavior of the cluster. Namely, interpuff intervals tend to be longer after large puffs and puffs tend to be smaller after short intervals. Numerical simulations of the dynamics of intracellular Ca^{2+} in the vicinity of a localized Ca^{2+} source show that very soon ($\sim 6\,\mathrm{ms}$) after Ca^{2+} release stops, the $[Ca^{2+}]$ becomes spatially homogeneous, particularly within a region the size of an IP_3R cluster [43]. In accordance with this observation, simulations performed for current amplitudes within the expected values for puffs [8] show a very weak dependence of $[Ca^{2+}]$ on this amplitude $\sim 6\,\mathrm{ms}$ after the current has stopped. Given the large size of the oocyte, we expect the value of $[Ca^{2+}]$ to be very close to the basal concentration ($\sim 50\,\mathrm{nM}$) a time $\sim 6ms$ after the termination of an isolated puff. This implies that for puffs as those analyzed in [55] Ca^{2+} exerts its inhibiting role during the puff or immediately upon puff termination. Taking these considerations into account we have based the effective cluster model on the diagram of Fig. 1. Namely, we have assumed that the cluster can exist in one of four different states: C–closed; O–open; I_1–inhibited 1; and I_2–inhibited 2. The various transition rates are chosen so that the model agrees with the available experimental evidence [55], but the functional forms are themselves arbitrary. This model does not take into account the dynamics of IP_3 binding and unbinding explicitely. This is so because, according to most IP_3R kinetic models, these processes are much faster than those related to calcium [44]. Thus, IP_3 bound and IP_3 free binding sites may be assumed to be in equilibrium between themselves. In this way, the effect of $[IP_3]$ can be taken into account by rescaling some of the transition rates of the model. In particular, we consider that the transition rate from C to O, k_{CO}, is an increasing function of $[IP_3]$. In this paper we assume that $[IP_3]$ is constant and uniform for each experiment so that we use a constant value for this rate.

Cytosolic Ca^{2+} also modulates the dynamics of single IP_3R's and, thus, of the cluster as a whole. We take this influence into account by assuming that some of the transitions between states and the total current depend on the $[Ca^{2+}]$ averaged over the region of the cluster ($\sim$ hundreds of nanometers). To include the activatory and inhibitory roles of Ca^{2+} we assume that both k_{CO} and k_{OI_1} are increasing functions of $[Ca^{2+}]$. To account for the different timescales of inhibition depending on puff amplitude, we assume that k_{OI_2} is independent of $[Ca^{2+}]$ and that the mean lifetime of I_1 is longer than that of I_2. In this way, for large values of $[Ca^{2+}]$ the transition from O to C is more likely to occur through I_1 which typically takes much longer than going through I_2. The fact that the transitions are irreversible and that the system must go to C before it can reopen allows us to separate these two types of behavior quite easily. The inclusion of the state I_2, on the other hand, allows us to regulate the rate of reopenings after a low amplitude puff. Given that IP_3R's need IP_3 to become open and that at small values of $[Ca^{2+}]$ the probability per unit time that they open is larger than they become inhibited, we assume that $k_{CO} = \hat{k}_{CO}([IP_3])\,[Ca^{2+}]$ and $k_{OI_1} = \hat{k}_{OI_1}\,[Ca^{2+}]^3$ where $\hat{k}_{CO}([IP_3])$ is an increasing function of $[IP_3]$. In this way, $[IP_3]$ regulates the excitability of the system, whereas $[Ca^{2+}]$ plays a dual role as it does for individual IP_3R's, increasing the transition rate from the closed to the open state and, at relatively large values of $[Ca^{2+}]$, the rate of inactivation through a transition to the state I_1. As we describe later, we investigate the model as depicted in Fig. 1 and variants in which the transition out of the O state is chosen differently but where k_{OI_1}/k_{OI_2} still rules the fraction of times it goes from O to I_1 as compared to I_2. In these variants, the mean open time of the cluster is independent of k_{OI_1} and k_{OI_2} and is not affected by their funcional forms.

B. Calcium current

Once the cluster makes a transition to its open state, we choose a random value for the current that depends on the value of $[Ca^{2+}]$ averaged over the region of the cluster immediately before the transition takes place. We have chosen this dependence so as to reproduce the results of the analysis of [55]. The experiments of [55] give values of the fluorescence amplitude rather than of the Ca^{2+} current. The observed fluorescence amplitude at each point and time, F, is linearly related to the Ca^{2+}-bound dye concentration, $[CaB]$, as:

$$[CaB] = [B]_T \frac{F - F_{min}}{F_{max} - F_{min}}, \quad (1)$$

where $[B]_T$ is the total dye concentration, F_{max} is the fluorescence under saturating dye conditions and F_{min} is the fluorescence of the Ca^{2+}-free dye. This is the first step in the algorithm we have developed to determine the current that underlies fluorescent images [56]. Application of this algorithm to Ca^{2+} puffs observed in oocytes [8] yields current values between 0.1 and 1.2pA and shows that puff amplitudes increase nonlinearly with the underlying current. However, the nonlinearity is weak and is only relevant for currents above 0.8pA, which are very rarely observed. Thus, for the sake of simplicity, we assume that the amplitude of each puff is linearly related to both the Ca^{2+} current and the maximum value of the underlying $[Ca^{2+}]$ averaged over the region of the cluster.

A word of caution is necessary here since $[Ca^{2+}]$ (and therefore, $[CaB]$ and F) not only depends on the underlying current. There are buffers in the cell (endogenous under physiological conditions both endogenous and exogenous in optical experiments) that interfere with the calcium distribution. The experiments analyzed in [55] were done in the presence of the slow exogenous buffer, EGTA. Taking into account the analyses of [57] we expect this buffer not to interfere (at least, significantly), with Ca^{2+}-mediated channel coupling between channels of the cluster or with the subsequent inhibitory effect of the released Ca^{2+}. Therefore, we expect it not to affect the values of the transition rates of the effective cluster model. We also expect that the amount of dye used did not affect those rates either. Fast or stationary buffers, however, could interfere with CICR and Ca^{2+}-inhibition within the cluster [57, 58]. The main assumption that underlies our approach is that the effects of endogenous buffers at the single cluster level can be incorporated into the transition rates of the effective cluster model. The hope is that the influence of other buffers that are subsequently added may be accounted for through their effect on the value of $[Ca^{2+}]$ within the cluster without altering the kinetic reaction rates. In this way the effective cluster model could be used to analyze the behavior of signals in the presence of different amounts of buffers. We will analyze this possibility in the future. The present paper treats buffers in the simplest possible way. Namely, we follow the same approach as in the original fire-diffuse-fire model [51] which considers that the effect of buffers is to rescale $[Ca^{2+}]$ and its diffusion coefficient. We will relax this simplification in the future and analyze to what extent it is possible to decouple the effective cluster model from the presence of different types of buffers in the cell.

The studies of [55] show that, due to the Ca^{2+} inhibitory effect, the amplitude of a puff at a site is smaller the smaller is the previous inter-puff time interval. This last quantity is of the order of a second for the experiments analyzed in [55]. As we have already mentioned, the Ca^{2+} concentration after such a long time is mainly determined by the time that has elapsed since the end of the release. Thus, in the model, we take into account the dependence between the amplitude of a puff and the previous inter-puff interval by assuming that the value of A (the $[Ca^{2+}]$ at the cluster upon its transition to the open state) is more likely to be large the smaller is u (the averaged $[Ca^{2+}]$ within the cluster) immediately before the occurrence of the transition. Numerical puff simulations performed with the algorithm of [43] show that the observed puff amplitude distributions analyzed in [8] may be reproduced using clusters that are $500nm \times 500nm$ in size and channels that open and close stochastically with a 0.1pA single channel current. The simulations of [43], which include buffers explicitely, show that the free Ca^{2+} concentration reaches values between 1 and $40\mu M$ at distances within $180nm$ of a 0.1pA point source and that the maximum value of $[Ca^{2+}]$ is about $60\mu M$ in the presence of a cluster with 20 channels that open and close stochastically. Taking these observations into account and considering that the $[Ca^{2+}]$ that enters the transition rates of the scheme of Fig. 1 is the average concentration over the whole cluster, we assume that it can take on values between 5 and $20\mu M$ during the occurrence of a puff. Furthermore, we assume that these two values correspond to the two extreme puff amplitude values of the experimental data that we use to choose the transition rates of the scheme of Fig. 1. Therefore, we relate A and u as follows:

$$\begin{aligned} A &= A_{max} - \frac{15\,\mu\mathrm{M}}{\frac{0.0017\,\mu\mathrm{M}}{r} + 1}, \quad \text{if } u - u_b > 0, \\ A &= A_{max}, \quad \text{if } u - u_b = 0, \end{aligned} \quad (2)$$

where r is a random variable that is uniformly distributed between 0 and $2(u - u_b)$. Eq. (2) guarantees that A varies between $5\mu M$ and $20\mu M$, that it is more likely to take on values that are closer to $20\,\mu$M as $u - u_b$ gets smaller and that it is independent of $[IP_3]$ as observed experimentally [8, 59].

For the determination of the transition rates of the kinetic model we work with Eq. (2) with $A_{max} = 20\,\mu$M. For the simulations of the stochastic fire-diffuse-fire model we need, instead, the number of Ca^{2+} ions that are released per unit time during each release event, σ (which is proportional to the Ca^{2+} current). We must stress that in this paper we are not modeling the buffer dynamics explicitely. We assume that their effect is to rescale the Ca^{2+} concentration and diffusion coeffi-

cients. Therefore, we work with a rescaled Ca^{2+} current too. Furthermore, since we will consider that each cluster is represented by a point source, we assume that $[Ca^{2+}]$ and σ are related by: $[Ca^{2+}]= \alpha\sigma/4\pi Dr$ where $\alpha = 1.66\,10^{-3}\,\mu m^3 \mu M$ is a unit conversion factor that guarantees that $[Ca^{2+}]$ is in μM when lengths are in μm. Thus, the Ca^{2+} amplitude, A, is given by:

$$A = \frac{1}{\frac{4}{3}\pi\,(\Delta r)^3}\int_0^{\Delta r}\frac{\alpha\sigma}{4\pi Dr}4\pi r^2 dr = \frac{3}{8\pi D\Delta r}\alpha\sigma, \quad (3)$$

where D is the Ca^{2+} effective diffusion coefficient and Δr is the grid size of the simulations.

C. Effective cluster model and puff duration

For fixed values of k_{OI_1} and k_{OI_2}, the open time distribution of a model in which transitions from the open state to others occurs directly as depicted in Fig. 1 is an exponential of mean $1/(k_{OI_1} + k_{OI_2})$. The experiments of [60] show that the distribution of blip durations can be fitted by a single exponential of time constant $\sim$ 17ms while the puff duration distribution is unimodal with a maximum at twice or three times the blip duration (see their Fig. 5). In [60] puff duration was computed as the time it takes for the observed fluorescence to go from its peak value during the puff to the basal level. The studies of [8], on the other hand, show that the duration of Ca^{2+} release during puffs ranges between 5 and 33ms and its distribution is also unimodal with mean $\sim$ 18ms. These results were obtained by application of the algorithm of [56] to linescan confocal experiments with temporal resolution limited by the linescan duration which was either 8 or 2.6ms. As shown in [60] and discussed in [8] puff or Ca^{2+}-release durations depend on the number of channels that open during each puff. The distribution of open channels, on the other hand, is non-monotonic too [60]. The latter can be explained in terms of the competition between Ca^{2+}-mediated inter-channel communication in the cluster and IP_3 binding [61]. Furthermore, depending on the relative weight between both processes, the distribution of the number of channels that open during a puff can change from being almost exponential to having a local maximum. The exponential distribution can be obtained when the number of IP_3R's with IP_3 bound is so small that they are sparsely distributed within each cluster. For the values of $[IP_3]$ that elicit Ca^{2+} waves we may expect the distribution of the number of channels that open during a puff to have a local maximum. Considering this non-monotonic distribution and both the inter-cluster and inter-channel variability, it is reasonable that both the puff and Ca^{2+}-release durations have distributions that are non-monotonic.

As mentioned before, for a model in which the transition from the open to the inhbited states occurs directly as in Fig. 1 with fixed values of k_{OI_1} and k_{OI_2} the distribution of open times is a single exponential, which is monotonic. As already explained, we consider k_{OI_1} to be a function of $[Ca^{2+}]$ which leads to open times that depend on puff amplitude. Given that the amplitude distribution that we obtain with the model is non-monotonic (see Fig. 2) we could expect the open time distribution to be non-monotonic too. In any case, to simplify the construction of the model we first determine the parameters of Fig. 1 so as to reproduce the observed distribution of inter-puff times considering that the transitions from O to I_1 and I_2 occur with probabilities per unit time, $k_{OI_1} = \hat{k}_{OI_1}[Ca^{2+}]^3$ and k_{OI_2}, respectively. Given the constraints that we impose to determine the parameters, we expect this approach to fix the range of values that the ratio k_{OI_1}/k_{OI_2} can take on (which is a function of the values that $[Ca^{2+}]$ can attain), but not the values that $\hat{k}_{OI_1}$ and k_{OI_2} can take on separately. We show later that this is the case by comparing the open time distributions obtained with this model and with others in which we change the way the cluster leaves the open state, but keep the fraction of times it goes to state I_1 to the number of times it goes to state I_2 always equal to $\hat{k}_{OI_1}[Ca^{2+}]^3/k_{OI_2}$.

III. CHOICE OF MODEL PARAMETERS BASED ON OBSERVED INTER-PUFF TIME DISTRIBUTIONS

The experiments analyzed in [55] consist of sequences of puffs that occur at the same site for a given value of $[IP_3]$. In order to determine the transition rates of the effective cluster model based on the behavior of the puff amplitudes and inter-puff time intervals observed in these data we need to model the Ca^{2+} dynamics between puffs. In this Section we do it in a very simple way. We assume that while the cluster is not releasing calcium (it is closed or inhibited), u (the $[Ca^{2+}]$ averaged over the cluster region) decays linearly during a short time $\sim t_d \sim 1\,$ms until it reaches a value $u_d = 0.42\,\mu$M and then approaches its basal level, $u_b = 40\,$nM following a power law [43]:

$$\begin{aligned} u(t) &= u(t) - \frac{u(t_e) - u_d}{t_d} \times (t - t_e), \\ &\qquad \text{if } t_e \le t \le t_e + t_d \\ u(t) &= (u_d - u_b) \times \left(1 + \frac{t - t_d}{\tau}\right)^{-\beta} + u_b, \\ &\qquad \text{if } t_e + t_d \le t_b, \end{aligned} \quad (4)$$

with u_d =0.42μM, t_d =6$\times 10^{-3}$s, β=0.65, τ=0.9$\times 10^{-3}$s and where t_e and t_b are two subsequent times at which Ca^{2+} release from the cluster ends and begins, respectively. The constants that appear in Eq. (4) were obtained by fitting this expression to the result of a numerical simulation of the reaction-diffusion system that models the dynamics of cytosolic Ca^{2+} in the presence of exogenous and endogenous buffers as described in [43] but in the presence of a 0.4 pA point source that remains

open during 10 ms and a Ca^{2+} pump as the one used in Section V. The validity of this type of approximation has been tested in [43].

We combine the effective cluster kinetic model of Fig. 1 with the interpuff Ca^{2+} dynamics of Eq. (4) to generate sequences of puff amplitudes separated by interpuff intervals. We do so with extensive numerical simulations in which the transitions between states of the release unit are modeled stochastically. In order to compare the results of the simulations with the experimental data analyzed in [55] we compute in both cases the accumulated distribution functions of different quantities of interest. We then compute the Kolmogorov statistics:

$$T \equiv \sup_x |F_1(x) - F_2(x)|, \tag{5}$$

where F_1 and F_2 are the experimental and model accumulated distribution functions, respectively. The statistical significance (p-values) of the differences between distributions is determined from look-up tables [62]. In the experiments, different release sites span different puff amplitude ranges. As done in [55] we grouped the experimental data in two sets according to the maximum amplitude observed at each site. All analyses presented here are based on events from the small cluster group.

We adjusted the parameters of the effective cluster model so as to minimize the value of T defined in Eq. 5 with F_1 and F_2 the experimental and the model interpuff time distributions, respectively. To this end we defined intervals of variation for each parameter of the effective cluster model. In each case, the borders of the interval differed by $\pm 40\%$ with respect to the mean. We then simulated the model for 3125 different combinations of the parameters and chose the one that produced the smallest value of T. The obtained parameters are listed in table I.

Parameter	Value
$\hat{k}_{CO}$	18.6 $\mu M^{-1} s^{-1}$
$\hat{k}_{OI_1}$	0.05 $\mu M^{-3} s^{-1}$
k_{OI_2}	40 s^{-1}
k_{I_1O}	0.7 s^{-1}
k_{I_2O}	2 s^{-1}

TABLE I: Parameter values of the kinetic model of Fig. 1 that minimize the Kolmogorov statistics (Eq. (5)) corresponding to the accumulated interpuff time distribution ($T = 0.078$, $p > 0.17$) where $k_{CO} = \hat{k}_{CO}([IP_3])$ $[Ca^{2+}]$ and $k_{OI_1} = \hat{k}_{OI_1}$ $[Ca^{2+}]^3$. We assume that $\hat{k}_{CO}([IP_3])$ is an increasing function of $[IP_3]$ so that the value obtained here corresponds to the $[IP_3]$ of the experiments used for the fitting. Only the ratio $\hat{k}_{OI_1}/k_{OI_2}$ can be determined from the fitting. We thus explore other possibilities that keep this ratio constant.

IV. ABILITY OF THE CLUSTER MODEL TO REPRODUCE OBSERVED PUFF PROPERTIES

To check that the model reproduces the interpuff time distribution that was used for the fitting and to test its ability to reproduce other features of the experimentally determined distributions not enforced with the fitting, we performed numerical simulations using the parameters shown in Table I and computed other distributions.

A. Puff amplitude and interpuff time distributions

Histograms of puff amplitude, A, and interpuff time, τ, obtained with the model are shown in Fig. 2. These figures are to be compared with Fig. 3 of [55]. Both for the model and the experiments the interpuff time distribution is concentrated within the range $\tau \leq 8s$. The maximum of the distribution occurs at $\tau \approx 1.5s$ in both cases and the standard deviation is $\sigma = 1.37s$ for the experiments and $\sigma = 1.81s$ for the model. Regarding the amplitude distribution, we must note that the scale of A differs between model and experiments. In the experiments the amplitude is given in terms of fluorescence, while in the model it given in terms of the averaged $[Ca^{2+}]$. Given our model assumptions, both quantities only differ by a proportionality constant. The experimental puff amplitudes vary between 0.05 and 0.2 while the range of variation of the model amplitudes is $5 - 20\,\mu$M so that the proportionality constant is $100\,\mu$M. Both distributions are asymmetrical with maxima occurring at $A = 0.1$ for the experiments and around $A = 10\mu M$ for the model. The standard deviations are 0.032 and $3.27\mu M$, respectively.

B. Conditional distributions

The conditional time and amplitude distributions obtained with the model are shown in Figs. 3 and 4. These figures are to be compared with Fig. 4 and 5 of [55]. The value ranges for the conditioning were chosen so that the conditioned variable was smaller than the first quantile or larger than the third quantile of the corresponding distribution in each case. These ranges differ slightly between model and experiment. Fig. 3 (a) is the amplitude distribution of puffs for which the preceding interpuff time is less than 1.01s and Fig. 3 (b) the one for which it is larger than 3.13s. In the case of the experiment, the conditioning corresponds to preceding interpuff times that are less than 1.4s and larger than 3.27s, respectively. Both for the model and the experiments the distribution conditioned to large interpuff times is concentranted around larger amplitude values than the one conditioned to smaller interpuff times with peaks occurring at $A \approx 12\mu M$ and $A \approx 8\mu M$ for the model and around 0.08 and 0.12 for the experiments. Fig. 4 (a) is the distribution of interpuff times that follow a puff with amplitude less than $9.21\mu M$ and Fig. 4 (b) the one for which the preceding

amplitude is larger than $13.76\mu M$. In the case of the experiment, the conditioning corresponds to preceding puff amplitudes that are less than 0.092 and larger than 0.134, respectively. Both for the model and the experiments the distribution conditioned to large puff amplitudes is concentranted around larger interpuff times than the one conditioned to smaller puff amplitudes with peaks occurring at $\tau \approx 1s$ and $\tau \approx 2s$ for the model and around 1s and 3s for the experiments.

C. Open time duration

We show in Fig. 5 (a) the open time, τ_o, distribution obtained with the model of Fig. 1 using the parameters of Table I. The distribution is monotonic with mean $\sim 8.73ms$ and standard deviation $\sim 11ms$. This differs from the distribution of Ca^{2+} release durations determined from experiments [8] which is unimodal and spreads between 5 and 33ms with mean $\sim$ 18ms. As mentioned before, we expect the fitting of the previous Section to only fix the ratio $\hat{k}_{OI_1}/k_{OI_2}$. If this is so, we can choose the open time duration from an *ad hoc* distribution that reproduces the experimental observations better and then decide to which of the two inhibited states it makes the transition from the open state keeping the ratio as given by Table I. With this aim, we have studied various models that only differ from the original one of Fig. 1 in the probability of leaving the open state: a model with $\hat{k}_{OI_1} = 0.005$ $\mu\text{M}^{-3}\text{s}^{-1}$ and k_{OI_2}= 4 s^{-1} instead of the values of Table I, a model in which the open time duration of each event is chosen from an exponential distribution with mean proportional to puff amplitude (equal to $6A/\mu$Mms) and another one in which it is chosen from a Gaussian distribution of mean 18 ms and a 7ms standard deviation. The exponential distribution has been selected based on the observation that puff duration is a (weakly) increasing function of the number of open channels (and, thus, of puff amplitude) [60]. The Gaussian one has been chosen to mimic the distribution of Ca^{2+} release durations determined in [8]. We also explored the behavior of the model of Fig. 1 with parameters given by Table I but for which events that lasted less than 2ms were discarded. The motivation in this case is to determine the effect of being unable to observe the shortest events on the interpuff time distritution and, therefore, on the parameters that we can estimate from the fitting. We show the open time distributions that correspond to some of these models in Fig. 5: (a) corresponds to the model of Fig. 1 and parameters as in Table I, (b) is similar to (a) but where events that lasted less than 2ms were discarded, (c) corresponds to the case in which the open duration is withdrawn from the amplitude dependent exponential distribution and (d) to the case in which it is taken from the Gaussian distribution already described. We show in Fig. 6 the interpuff time distributions obtained from simulations performed using these models. We observe that the distributions in (c) and (d) are undistinguishable from the one obtained with the model of Fig. 1 and parameters as in Table I (shown in (a)). A similar behavior is obtained for the model with $\hat{k}_{OI_1} = 0.005$ $\mu\text{M}^{-3}\text{s}^{-1}$ and k_{OI_2}= 4 s^{-1} (data not shown). The mean values and standard deviations of the amplitude and inter-puff times obtained with these models are all very similar as shown in Table II. We then conclude that all these models reproduce equally well the sole distribution that was used to fix the parameter values that characterize the transitions between states (all but the individual values of $\hat{k}_{OI_1}$ = and k_{OI_2}). The interpuff time distribution for the original model but in which events that are shorter than 2ms have been discarded is shown in Fig. 6 (b). We see that is only slightly different from the one in Fig. 6 (a). Therefore, we do not expect the inability to observe the shortest events to alter much the transition rates of Table I.

Model	A (μM)	τ (s)	τ_o (ms)
Original	11.4, 3.3	2.1, 1.8	8.7, 11
Exponential	11.4, 3.3	2.1, 1.8	66, 74
Gaussian	11.4, 3.3	2.1, 1.8	17.3, 6.9
Slow original	11.5, 3.3	2.1, 1.8	94, 108
Cropped original	10.9, 2.7	2.7, 2.7	11.2, 11.4

TABLE II: Mean and standard deviations of [Ca^{2+}] amplitude, A, inter-puff time, τ, and open state duration, τ_o, obtained combining the interpuff Ca^{2+} dynamics of Eq. (4) with stochastic simulations of the model of Fig. 1 for various choices of the open time distribution. Original corresponds to considering that the transitions from O to I_1 and I_2 occur, respectively, with probabilities per unit time $k_{OI_1} = \hat{k}_{OI_1}[Ca^{2+}]^3$ and k_{OI_2} with the parameters of Table I. Exponential corresponds to a model in which the open time duration of an event of amplitude, A, is withdrawn from an exponential distribution of mean $6A/\mu$Mms. Gaussian corresponds to a model in which the open time duration is withdrawn from a Gaussian distribution of mean 18 ms and a 7ms standard deviation. Simulations for the slow original model only differ from the original one in the values of $\hat{k}_{OI_1}$ and k_{OI_2} which are equal to 0.005 $\mu\text{M}^{-3}\text{s}^{-1}$ and 4 s^{-1}, respectively. Simulations for the cropped original model are obtained using the original model and discarding open events that last less than 2ms.

The agreement between model and experiments at the level of the amplitude and conditional distributions displayed in Figs. 2–4. is very good and goes beyond the information that was used to choose the transition rates. The open time distribution, on the other hand, can be chosen as needed to reproduce the observations as long as the fraction of transitions from the open state to one or the other inhibited ones is kept as given by Table I. We thus conclude that the model of Fig. 1 provides a skeleton that captures the basic behavior of the observations and, combined with a proper open time distribution, is able to reproduce all of them quantitatively.

V. STOCHASTIC FIRE-DIFFUSE-FIRE MODEL

In this Section we describe how we construct the stochastic "fire-diffuse-fire model" using the heuristic cluster model developed before. As in [49–51], we consider a one dimensional medium with equally spaced point sources separated by a distance d. Each of these sources represents a cluster of IP_3R's. Their dynamics is ruled by the kinetic model of Fig. 1. Ca^{2+} ions diffuse in the medium with coefficient D and are recaptured by pumps. $[Ca^{2+}]$ is then a function of one spatial coordinate, x, and time, t. The same type of description applies for plane waves that propagate in three dimensions along the x direction. The original "fire-diffuse-fire model" was introduced to understand the properties of the wave front along the direction of propagation and the description was limited to plane waves. One of our main motivations now is to apply the stochastic fire-diffuse-fire model to describe the propagation of Ca^{2+} signals in quasi-one dimensional regions such as neuron spines. The spatiotemporal evolution of the calcium concentration $u(x,t) \equiv [Ca^{2+}]$ is then given by:

$$\frac{\partial u}{\partial t} = D\nabla^2 u + \sum_{i=-\infty}^{+\infty} \frac{\alpha\sigma_i(t)}{A_t}\delta(x-id) - \frac{v_p u^2}{u^2+k_p} + \frac{v_p u_b^2}{u_b^2+k_p} \tag{6}$$

where $\sigma_i(t)$ is the number of Ca^{2+} ions released at site i per unit time at time t, α is the unit conversion factor introduced before and A_t represents the area of the cluster. $\sigma_i = 0$ if the release site is in a closed or inactive state. When the cluster at the i-th site makes a transition to the open state the random value of σ_i is chosen combining Eqs. (2) and (3). It remains constant while the cluster stays open. The transitions between states of each release unit occur stochastically following the kinetic scheme of Fig. 1 where $[Ca^{2+}]$ is the time-dependent concentration at the grid point where the site is located. As mentioned before, σ_i and D are effective currents and diffusion coefficients, respectively. This is the way in which we take into account the presence of buffers in this paper. The third term in Eq. (6) describes the action of the Ca^{2+} ATPase that pumps free Ca^{2+} ions from the cytosol into the endoplasmic reticulum which we model as in [44] with $v_p = 0.9\,\mu\mathrm{Ms}^{-1}$ and $k_p = 0.01\,\mu\mathrm{M}^2$. The last term in Eq. (6) represents the leak from the ER that has been chosen so as to compensate the action of the pumps at the basal level, $u_b = [Ca^{2+}]_{basal}$.

We simulate Eq. (6) using a forward Euler method in time with time step $dt = 50\,\mu$s, an explicit finite-difference formula in space with a second order expression for the Laplacian and grid spacing $\Delta x = 0.1\,\mu$m. The boundary conditions are no-flux. We simulate the stochastic transitions between states of the cluster discretely in time with the same time step, $dt = 50\,\mu$s. Initially, $[Ca^{2+}]$ is at its basal level $u_b = 0.04\,\mu$M and all the release units are at the closed state, C. For the transition rates we first use all the parameters of Table I except for $\hat{k}_{CO}$ which we vary to simulate situations with different $[IP_3]$. The results of Fig. 7 correspond to simulations obtained with $D = 20\,\mu\mathrm{m}^2/\mathrm{s}$, $A_t = 0.2\,\mu\mathrm{m}^2$ and 15 release sites separated by $d = 2\,\mu$m. The sites are placed in the middle of a $50\,\mu$m domain so as to guarantee that the borders play no role. Regarding the parameters that characterize the release currents we use $A_{max} 50\,\mu$M in Eq. (2), which is larger than before, because the region over which A is computed in Eq. (3) has smaller longitudinal extent than that of a cluster. In this case, the values that each σ_i can take on vary within the range $[3.5\text{–}5]10^5 \mathrm{ions\ s}^{-1}$ which correspond to currents between 0.11pA and 0.16pA. These values for the effective Ca^{2+} current are consistent with an 86% buffering or less given that puff currents have been estimated to range between 0.1 and 1.2pA [8].

The aim of the simulations we show here is to illustrate that the model is able to display transition regimes between different forms of propagation as the excitability of the medium is increased. In this way we try to reproduce the type of signals observed experimentally as $[IP_3]$ is increased. The observations that we seek to mimic are obtained by injecting caged IP_3 in the cell and subsequently releasing it with a UV flash. One of the drawbacks of this approach is that the exact value of $[IP_3]$ achieved at each instance is unknown. However, it is clear that small values of $[IP_3]$ give rise to localized signals while larger values are necessary to elicit waves. The only parameter of our heuristic cluster model that we assume depends on $[IP_3]$ is $\hat{k}_{CO}([IP_3])$. Furthermore, we assume that it increases with $[IP_3]$. Therefore we seek to reproduce the experimental observations that correspond to different values of $[IP_3]$ by changing the value of $\hat{k}_{CO}$. We show the result of such simulations in Fig. 7 where $\hat{k}_{CO}$ increases from left to right. Only puffs are found at low values, *i.e.*, release events are localized and not coordinated on a length scale of several cluster spacings. At slightly higher values the release sites start to couple. Further increasing $\hat{k}_{CO}$ (or, equivalently, $[IP_3]$) leads to global waves that travel across a large region. In the simulation with $\hat{k}_{CO} = 15\,\mu\mathrm{M}^{-1}\mathrm{s}^{-1}$ the site in the middle of the domain starts to release Ca^{2+} at $t = 0$ and all sites to its right subsequently fire with the seven-th site to its right (located a distance $12\,\mu$m from the middle) firing at $t \approx 0.6\,$s. This corresponds to a speed $\sim 20\,\mu$m/s. In the simulation with at $\hat{k}_{CO} = 45\,\mu\mathrm{M}^{-1}\mathrm{s}^{-1}$ all sites to the left of the middle one fire within $\sim 0.45\,$s which corresponds to a speed $\sim 27\,\mu$m/s. We then conclude that the model is able to generate simulations in which the speed increases with $\hat{k}_{CO}$ within values that are similar to those of saltatory waves [63].

In the previous Section we studied a variety of models which main difference with respect to the one used for the simulations of Fig. 7 is the way the Ca^{2+} release duration is chosen. We show in Fig. 8 that these models are also able to display transition regimes with wave speeds that vary within the same range. We show in Fig. 8 (a) and (b) simulations obtained with the "slow original model"

(a version of the original model in which $\hat{k}_{OI_1} = 0.005$ $\mu\mathrm{M}^{-3}\mathrm{s}^{-1}$ and $k_{OI_2} = 4\ \mathrm{s}^{-1}$ instead of the values of Table I). We observe that already at $\hat{k}_{CO} = 1\mu\mathrm{M}^{-1}\mathrm{s}^{-1}$ the activity of different clusters is coupled via CICR. This differs from what we found with the original model at $\hat{k}_{CO} = 1\mu\mathrm{M}^{-1}\mathrm{s}^{-1}$ (see first frame of Fig. 7) and is due to the larger amount of Ca^{2+} ions that are released as the cluster remains open for a larger time. Because of the same reason, the velocity of the Ca^{2+} wave that can be elicited at $\hat{k}_{CO} = 15\mu\mathrm{M}^{-1}\mathrm{s}^{-1}$ is larger in Fig. 8 ($\sim 34\,\mu$m/s for the front that goes from $x = 15\,\mu$m to $x = 21\,\mu$m in the figure) than in the second frame of Fig. 7 ($\sim 20\,\mu$m/s as described before). We show in Figs. 8 (c) and (d) simulations obtained with the model in which the open duration is drawn from a Gaussian distribution. In this case we are able to obtain similar transitions to those of the original model with smaller current amplitude values ($A_{max} = 30\,\mu$M in Figs. 8 (c) and (d) and $A_{max} = 50\,\mu$M in Figs. 7). The speeds of propagation obtained for $\hat{k}_{CO} = 45\mu\mathrm{M}^{-1}\mathrm{s}^{-1}$ are also similar for both models ($\sim 28\,\mu$m/s for the front that goes from $x = 19\,\mu$m to $x = 23\,\mu$m and $\sim 39\,\mu$m/s for the one that goes from $x = 19\,\mu$m to $x = 11\,\mu$m in Fig. 8 (d) while $\sim 27\,\mu$m/s in the last frame of Fig. 7 as described before). Similar conclusions may be drawn from simulations done using the other models tested in the previous Sections (data not shown). We then conclude that if the release duration is most of the times smaller than 30–40ms, as in the models considered here, the open time distribution itself does not affect the type of signal (which results saltatory). This is reasonable given that, for the largest speeds ($\sim 30\,\mu$m/s), the time it takes for the wave to travel between clusters is 70 ms. The speed, on the other hand, is mainly determined by the combination of the mean duration and the Ca^{2+} current since the resulting $[Ca^{2+}]$ affects both the probability that a cluster becomes open and the amplitude of the release event.

VI. DISCUSSION AND CONCLUSIONS

Intracellular Ca^{2+} signals are ubiquitous across cell types [1]. They can be localized or propagate throughout the cell [2]. In both cases, Ca^{2+} entry through specialized channels is involved. Therefore, the characteristic time and lengthscales of the processes that underlie global Ca^{2+} signals span several orders of magnitude. This poses great challenges from a modeling perspective and has led to the development of a variety of approaches as described in the Introduction. Furthermore, it is clear that stochasticity drives global Ca^{2+} signals. Even if many channels are open at any given time, the large concentration gradients that form around each of them prevent mean-field models to be an accurate description of the overall dynamics [31]. Efficient modeling strategies are necessary to include the intrinsic stochasticity of global signals describing, at the same time, the largest scales involved.

Ca^{2+} release from the endoplasmic reticulum through IP_3R's is a key component of the signaling toolkit. Many properties of IP_3R-mediated signals have been inferred from optical experiments, particularly, those performed in *Xenopus Laevis* oocytes. These experiments have provided evidence that IP_3R's are organized in clusters which are separated a few microns. Local (limited to one or a few open channels in a cluster) or global signals are elicited depending on the amount of IP_3. Global signals are the result of cluster-cluster interactions mediated by the Ca^{2+} ions that diffuse from one site to the other. Clusters of IP_3R's can then be viewed as the basic release unit of IP_3R-mediated signals. This is the approach we followed when we introduced the very idealized "fire-diffuse-fire" model [49–51]: a reaction-diffusion system for $[Ca^{2+}]$ with point sources representing IP_3R-clusters that became open if $[Ca^{2+}]$ at the site exceeded a threshold. One of the main drawbacks of this original proposal was the deterministic description of Ca^{2+} release. A stochastic version of the model was introduced in [52, 53] where the threshold was set to a random variable of a given distribution. In this paper we have used puff information to construct a (more realistic) phenomenological stochastic cluster model that we have subsequently used to describe the dynamics of Ca^{2+} release in a modified version of the "fire-diffuse-fire model". The idea of using IP_3R clusters as the basic Ca^{2+} release unit is one of the distinctive features of the model presented in [31]. In this case, a master equation for the cluster is derived based on an IP_3R kinetic model. Our approach is different: it builds the cluster model based on puff observations directly and fixes its parameter values so as to reproduce some statistics of these observations. In particular, we have used the inter-puff time distribution to determine the transitions rates among states and then used the puff amplitude and various contrained distributions to check the validity of the model. We have obtained very good agreement on these other distributions. We have shown that the distribution of times the cluster remains open can be subsequently chosen without affecting the ability of the model to reproduce both the constrained and unconstrained amplitude and inter-puff time distributions. Therefore, it can be fixed so that it reproduces the experimental observations. The effective cluster model is not strictly Markovian: there is not a fixed value of the $[Ca^{2+}]$ amplitude at the release site, A, or of the number of ions released per unit time, σ, associated to the open state, O. When the cluster makes a transition to O, a random value for A is chosen using Eq. (2) and σ is then derived by means of Eq. (3). Analogously, he open time duration may also be picked from an arbitrary (not necessarily exponential) distribution.

In this paper we have used the effective cluster model built in this way to simulate a variety of Ca^{2+} signals within the framework of the "fire-diffuse-fire" model. This involves several simplifications, among others, the geometry is one dimensional, IP_3R clusters are equally spaced and the interaction with buffers is taken into ac-

count through a rescaled diffusion coefficient and current. Its generalization to more dimensions and with a more realistic site distribution is immediate. The presence of buffers can be taken into account explicitely as usual by coupling the evolution equation for $[Ca^{2+}]$ to others for the various Ca^{2+}-bound buffer concentrations. In such a case, the free diffusion coefficient for Ca^{2+} would be used instead of the effective one in the $[Ca^{2+}]$ evolution equation and there would be additional terms related to the various Ca^{2+}-buffer reactions considered. The main question that arises is to what extent our effective cluster model depends on the specificities of the experimental situation that was used to fix its parameter values. In particular, whether the derived model would change in the presence of other exogenous or endogenous buffers. We think that the structure of the model should persist in most cases, keeping the particular dependence on $[Ca^{2+}]$ and $[IP_3]$ of the rates of transition between cluster states that we have considered. Let us assume that we use the cluster model that we have obtained to simulate a situation where buffers other than those that were present in the original experiments have been added. The addition of these buffers could affect the $[Ca^{2+}]$ within the cluster region and that would indirectly change the transition rates. The question is if this Ca^{2+}-mediated effect is enough to take into account the influence of these new buffers on the cluster dynamics. We think that it should be enough in the case of slow buffers. The case of fast buffers should be studied in more detail. A similar concern arises with respect to the dependence of the Ca^{2+} current on the averaged $[Ca^{2+}]$ before the onset of release (Eq. 2). We will analyze these issues in more detail in a future work. Regarding the released current, there is an additional aspect. As observed in [55] individual IP_3R's seem to remain inhibited for a relatively long time before they can reopen. Therefore, the number of IP_3R's of a cluster that are able to open at any given time depends on how many opened during the previous release event at the site and on the time elapsed since then. The decreasing dependence with $[Ca^{2+}]$ of the allowed values of the Ca^{2+} current given by Eq. (2) carries the implicit assumption that the averaged $[Ca^{2+}]$ provides information on the time elapsed since the previous release event. This is correct when $[Ca^{2+}]$ changes at a site are exclusively due to Ca^{2+} release from the same site, as in the experiments that were used to fit the parameters of the effective cluster model. In the case of the simulations of Fig. 7, having used $A_{max} = 50\mu M$ decreased the relative range of variation of the current values and made the effect of the Ca^{2+} induced inhibition less noticeable. This is reasonable in a model like the "fire-diffuse-fire" in which the aim is to study the response of each site the first time it "fires". In particular, we are planning to use the stochastic "fire-diffuse-fire" introduced here to study how the signal propagation properties change in the presence of different amounts and types of buffers and under the type of conditioning protocols that are applied to study synaptic plasticity. The performance of our effective cluster model within a more detailed description of the intracellular Ca^{2+} dynamics in which the clusters can "fire" several times needs a deeper analysis that will be the subject of a future work.

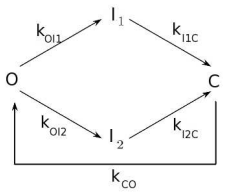

FIG. 1: Cluster kinetic model. The states and transitions were chosen so as to reproduce observed puff properties. When the cluster is in the closed, C, or inhibited states, I_1, I_2, there is no release. When it is in the open state, O, the release current or $[Ca^{2+}]$ amplitude is chosen from a distribution.

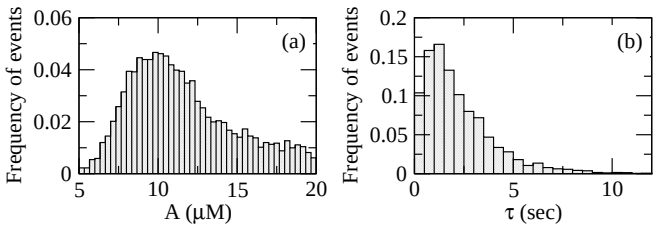

FIG. 2: Histograms of amplitude and interpuff times obtained combining stochastic simulations of the cluster kinetic model of Fig. 1 with the interpuff Ca^{2+} dynamics of Eq. (4) .

VII. ACKNOWLEDGMENTS

Acknowledgments

This research is supported by UBA (UBACyT X208), ANPCyT (PICT 17-21001), Santa Fe Institute, Fundación Antorchas and CONICET (PIP 5131). D.F. and S.P.D. are members of Carrera del Investigador Científico (CONICET).

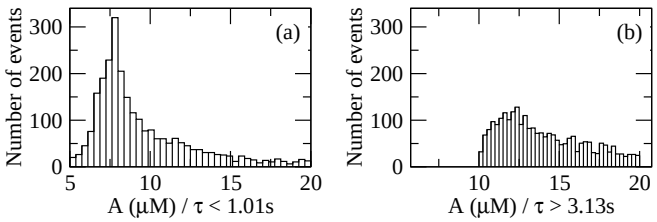

FIG. 3: Conditional distributions obtained with the same simulations as in Fig. 2. (a) Amplitude distribution of puffs for which the preceding interpuff time satisfies $\tau < 1.01\,\mathrm{s}$. (b) Similar to (a) but for $\tau > 3.13\,\mathrm{s}$.

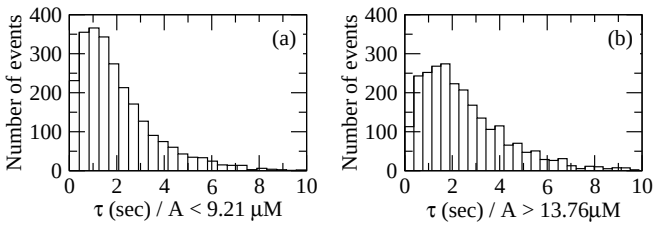

FIG. 4: Conditional distributions obtained with the same simulations as in Fig. 2. (a) Distribution of interpuff times for which the preceding puff amplitude satisfies $A < 9.21\,\mu$M . (b) S

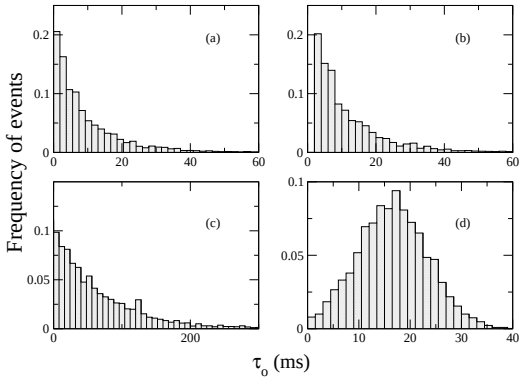

FIG. 5: Open time distributions obtained with the model of Fig. 1 and the parameters of Table I (a), with the same model as in (a) but for which events that lasted less than 2ms were discarded (b), with the exponential and the Gaussian models ((c) and (d), respectively).

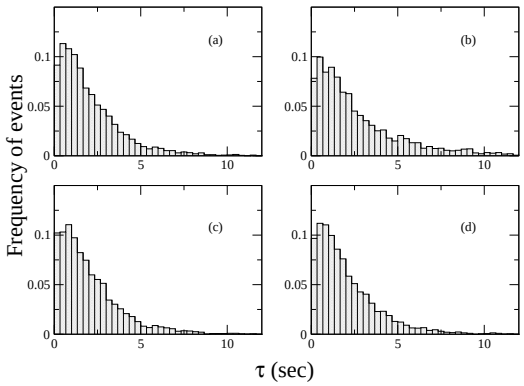

FIG. 6: Interpuff time distributions obtained with the same simulations as in Fig. 5

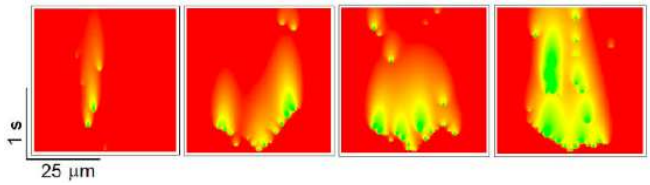

FIG. 7: (Color online) Space-time plots of $[Ca^{2+}]$ obtained with the stochastic fire-diffuse-fire model using, from left to right, $\hat{k}_{CO} = 1\,\mu\text{M}^{-1}\text{s}^{-1}$, $15\,\mu\text{M}^{-1}\text{s}^{-1}$, $30\,\mu\text{M}^{-1}\text{s}^{-1}$ and $45\,\mu\text{M}^{-1}\text{s}^{-1}$, respectively. The rest of the parameters are as in Table I. $[Ca^{2+}]$ is displayed with a color code that goes from red (low $[Ca^{2+}]$) to green (high $[Ca^{2+}]$) which shows as grey and white, respectively, in the grayscale printed version.

[1] M. J. Berridge, M. D. Bootman, and P. Lipp, Nature **395**, 645 (1998).
[2] Y. Yao, J. Choi, and I. Parker, J Physiol **482 (Pt 3)**, 533 (1995).
[3] M. J. Berridge, J Exp Biol **200**, 315 (1997).
[4] X. P. Sun, N. Callamaras, J. S. Marchant, and I. Parker, J Physiol **509 (Pt 1)**, 67 (1998).
[5] S. Swillens, G. Dupont, L. Combettes, and P. Champeil, Proc Natl Acad Sci U S A **96**, 13750 (1999).
[6] J. Marchant and I. Parker, EMBO J **20**, 65 (2001).
[7] J. Shuai, H. J. Rose, and I. Parker, Biophys J **91**, 4033 (2006).
[8] L. Bruno, G. Solovey, A. C. Ventura, S. Dargan, and S. Ponce Dawson, Cell Calcium **47**, 273 (2010).
[9] C. Taylor, Biochem. Biophys. Acta **1436**, 19 (1998).
[10] S. Patel, S. Joseph, and A. Thomas, Cell Calcium **25**, 247 (1999).
[11] M. Iino, J. Gen. Physiol. **95**, 1103 (1990).
[12] E. Finch, T. Turner, and S. Goldin, Science **252**, 443 (1991).
[13] I. Bezprozvanny, J. Watras, and B. E. Ehrlich, Nature **351**, 751 (1991).
[14] J. Ramos-Franco, M. Fill, and G. Mignery, Biophys. J. **75**, 834 (1998).
[15] D. Mak, S. McBride, and J. Foskett, Proc. Natl. Acad. Sci. USA **95**, 15821 (1998).
[16] N. Callamaras and I. Parker, Cell Calcium **15**, 66 (1994).
[17] D. O. Mak and J. K. Foskett, J Gen Physiol **109**, 571 (1997).
[18] J. W. Shuai and P. Jung, Proc Natl Acad Sci U S A **100**, 506 (2003).
[19] I. Parker and Y. Yao, J Physiol **491 (Pt 3)**, 663 (1996).
[20] M. Bootman, E. Niggli, M. Berridge, and P. Lipp, J Phys-

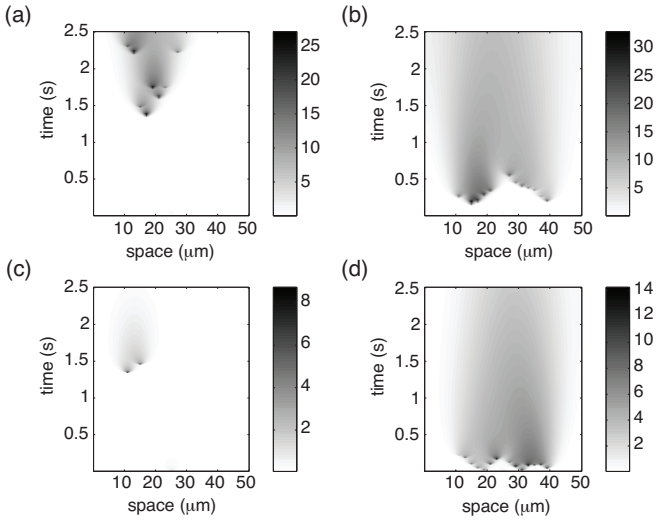

FIG. 8: Examples of Ca^{2+} signals obtained with simulations of the stochastic fire-diffuse-fire model for various versions of the cluster model that differ on the way the release duration of each event is determined: Slow original model with $A_{max} = 50\mu$M and $\hat{k}_{CO} = 1\mu\text{M}^{-1}\text{s}^{-1}$ (a) and with $A_{max} = 50\mu$M and $\hat{k}_{CO} = 15\mu\text{M}^{-1}\text{s}^{-1}$, Gaussian model with $A_{max} = 30\mu$M and $\hat{k}_{CO} = 1\mu\text{M}^{-1}\text{s}^{-1}$ (c) and with $A_{max} = 30\mu$M $\hat{k}_{CO} = 45\mu\text{M}^{-1}\text{s}^{-1}$ (d)

iol **499 (Pt 2)**, 307 (1997).

[21] I. Parker and Y. Yao, Proc Biol Sci **246**, 269 (1991).

[22] I. Parker, J. Choi, and Y. Yao, Cell Calcium **20**, 105 (1996).

[23] N. Callamaras, J. S. Marchant, X. P. Sun, and I. Parker, J Physiol **509 (Pt 1)**, 81 (1998).

[24] S. Swillens, P. Champeil, L. Combettes, and G. Dupont, Cell Calcium **23**, 291 (1998).

[25] S. Schuster, M. Marhl, and T. Hfer, Eur J Biochem **269**, 1333 (2002).

[26] J. W. Shuai and P. Jung, Biophys J **83**, 87 (2002).

[27] M. Falcke, Biophys J **84**, 42 (2003).

[28] D. Swaminathan, G. Ullah, and P. Jung, Chaos: An Interdisciplinary Journal of Nonlinear Science **19**, 037109 (pages 9) (2009), URL `http://link.aip.org/link/?CHA/19/037109/1`.

[29] A. Skupin, H. Kettenmann, U. Winkler, M. Wartenberg, H. Sauer, S. C. Tovey, C. W. Taylor, and M. Falcke, Biophys J **94**, 2404 (2008).

[30] A. Skupin, H. Kettenmann, U. Winkler, M. Wartenberg, H. Sauer, S. C. Tovey, C. W. Taylor, and M. Falcke, Biophys. J. **94**, 2404 (2008).

[31] R. Thul, K. Thurley, and M. Falcke, Chaos: An Interdisciplinary Journal of Nonlinear Science **19**, 037108 (pages 14) (2009), URL `http://link.aip.org/link/?CHA/19/037108/1`.

[32] M. Perc, A. K. Green, C. J. Dixon, and M. Marhl, Biophys. Chem. **132**, 33 (2008).

[33] M. Perc, M. Gosak, and M. Marhl, Chem. Phys. Lett. **437**, 143 (2007).

[34] M. Perc, M. Gosak, and M. Marhl, Chem. Phys. Lett. **421**, 106 (2006).

[35] H. DeRemigio and G. D. Smith, Cell Calcium **38**, 73 (2005).

[36] L. Diambra and N. Guisoni, Cell Calcium **37**, 321 (2005).

[37] G. Ullah and P. Jung, Biophys J **90**, 3485 (2006).

[38] J. Shuai and P. Jung, New Journal of Physics **5**, 132 (2003).

[39] R. Thul and M. Falcke, Biophys J **86**, 2660 (2004).

[40] M. Bar, M. Falcke, H. Levine, and L. S. Tsimring, Phys Rev Lett **84**, 5664 (2000).

[41] M. Falcke, L. Tsimring, and H. Levine, Phys Rev E Stat Phys Plasmas Fluids Relat Interdiscip Topics **62**, 2636 (2000).

[42] S. Rüdiger, J. W. Shuai, W. Huisinga, C. Nagaiah, G. Warnecke, I. Parker, and M. Falcke, Biophys J **93**, 1847 (2007).

[43] G. Solovey, D. Fraiman, B. Pando, and S. Ponce Dawson, Phys. Rev. E **78**, 041915: 1 (2008).

[44] G. W. De Young and J. Keizer, Proc Natl Acad Sci U S A **89**, 9895 (1992).

[45] D. Fraiman and S. P. Dawson, Cell Calcium **35**, 403 (2004).

[46] J. Shuai, J. Pearson, J. Foskett, D.-O. D. Mak, and I. Parker, Biophys. J. **93**, 1151 (2007).

[47] E. Gin, M. Falcke, L. E. Wagner, D. I. Yule, and J. Sneyd, Biophys J **96**, 4053 (2009).

[48] T. Ur-Rahman, A. Skupin, M. Falcke, and C. W. Taylor, Nature **458**, 655 (2009).

[49] J. Keizer, G. D. Smith, S. Ponce-Dawson, and J. E. Pearson, Biophys. J. **75**, 595 (1998).

[50] J. E. Pearson and S. Ponce-Dawson, Physica A **257**, 141 (1998).

[51] S. P. Dawson, J. Keizer, and J. E. Pearson, Proc Natl Acad Sci U S A **96**, 6060 (1999).

[52] S. Coombes and Y. Timofeeva, Phys. Rev. E **68**, 021915:1 (2003).

[53] Y. Timofeeva and S. Coombes, Phys. Rev. E **70**, 062901:1 (2004).

[54] K. Bentele and M. Falcke, Biophys J **93**, 2597 (2007).

[55] D. Fraiman, B. Pando, S. Dargan, I. Parker, and S. Ponce Dawson, Biophys. J. **90**, 3897 (2006).

[56] A. C. Ventura, L. Bruno, A. Demuro, I. Parker, and S. Ponce Dawson, Biophys. J. **88**, 2403 (2005).

[57] S. Zeller, S. Rdiger, H. Engel, S. Sneyd, G. Warnecke, I. Parker, and M. Falcke, Biophys J **97**, 992 (2009).

[58] J. Shuai, J. Pearson, and I. Parker, Biophys. J. **95**, 3738 (2008).

[59] H. J. Rose, S. Dargan, J. Shuai, and I. Parker, Biophys J **91**, 4024 (2006).

[60] I. F. Smith and I. Parker, Proc. Natl. Acad. Sci. (USA) **106**, 6404 (2009), URL `http://www.pnas.org/content/106/15/6404.full.pdf+html`.

[61] G. Solovey and S. Ponce Dawson, PLoS ONE **5**, e8997 (2010).

[62] W. Conover, *Practical Nonparametric Statistics* (Hoboken, N.J. : Wiley, 1998).

[63] J. Marchant, N. Callamaras, and I. Parker, EMBO J **18**, 5285 (1999).